# Location Determination of Transient Cable Fault by Graphical Analysis of Time-Domain Waveform with Impact of Load Distribution

Derrick S. Anang and Charles Kim, *Senior Member, IEEE*

***Abstract*— This paper is a continuation of fault location research specifically for self-clearing, transient, underground cable faults in power distribution systems. From the initial inverse time-domain approach to the graphical implementation of the algorithm, the focus has been an improvement in the accuracy of the algorithm in real situations. The primary focus of this paper is to investigate the influence of the fault location with respect to the load center location. Varied load configurations and load profiles are implemented to test the application and determine the flexibility, adaptability and accuracy of the graphically implemented algorithm. The tests involve the use of fault data generated from simulations under different multi-spatial loads in ATP/EMTP and a validation using preset cable parameters. The findings made from the study include a comparison of the results from faults at different sections along cables that lie in between loads. Initial observations are discussed with respect to the impact of varied load center locations.**

***Index Terms*— *Transient faults, 2D graphs, distribution system, underground cable, load profile, ATP/EMTP, line resistance, line inductance, fault location, multi-spatial loads.***

## I. Introduction

Predictive fault location has gained much interest in utility industry in an attempt to improve reliability of service by desired service continuity or reduced down-time through the said approach. However, the difficulties in realizing the approach lies in the fact that the self-clearing, transient fault lasts too short a time to apply conventional fault location algorithms. The conventional fault location algorithms, which are popularly implemented in distance relays, are principled on the changes in the line impedance before and after a fault. They further assume a steady-state post-fault; therefore, they take the decision parameters from the fundamental frequency components of the power system. The extraction of the fundamental components requires at least two steady-state cycles for frequency analysis. Therefore, this steady-state approach of the conventional fault location algorithms could not be applied to short-lived, self-clearing faults which last less than 1 power-cycle before returning back to normal state.

In solving self-clearing faults, we pioneered efforts by introducing a time-domain, inverse differential equation approach applied to a faulted loop [1], [2]. The essence of the initial approach is to apply a simple second-order differential equation on the faulted loop for a formulation with voltage injection at the fault location. Then, the superposition principle is applied to calculate the fault location in terms of inductance or inductive reactance. The superposition approach is extremely useful in fault location in a circuit feeder when a power monitor such as PQnode is installed in a bus which serves multiple circuits [3]-[4].

After the preliminary studies on locating self-clearing faults [1]–[4], an extensive field test has been performed with a slightly revised algorithm [5]. The revised algorithm now includes once ignored line resistance; therefore, the differential equation of faulted loop contains 2 unknowns - line resistance and line inductance to the fault. The revised algorithm applies two approaches in solving one differential equation with two unknowns: (a) Zero-crossing point approach and (b) Least-Square Error (LSE) approach for parameter estimation.

In the zero-crossing approach, the inductance to the fault is determined from the inductance locus at the zero-crossing point(s) of the fault loop current. Similarly, the resistance to fault is determined from the resistance locus at the zero-crossing point(s) of the derivative of the fault loop current [5]. More specifically, for a simple *RL* circuit whose voltage equation is,

$$v(t) = R \cdot i(t) + L \cdot \frac{di(t)}{dt}$$

with known (or measured) $v(t)$ and $i(t)$, the inductance to the fault, *L*, can be written as

$$L = \frac{v(t) - R \cdot i(t)}{\frac{di(t)}{dt}}$$

Even with the known (measured) $v(t)$ and $i(t)$, there still remains an unknown component, *R*, resistance to the fault. But if $i(t) = 0$, then the unknown *R* is also eliminated from the *L* equation above. Therefore, at $i(t) = 0$, the fault distance in inductance can be determined by,

$$L = \left( \frac{v(t)}{\frac{di(t)}{dt}} \middle| i(t) = 0 \right)$$

Derrick S. Anang is a graduate student in Electrical Engineering and Computer Science at Howard University, Washington, DC 20059 USA (e-mail: derrick.anang@bison.howard.edu).

Charles Kim is with the Electrical Engineering and Computer Science Department, Howard University, Washington, DC 20059 USA (e-mail: ckim@howard.edu).

Similarly, $R$ can be determined by reading at $(\frac{di(t)}{dt}) = 0$ from the resistance locus equation of:

$$R = \left( \frac{v(t)}{i(t)} \middle| \left\{ \frac{di}{dt} = 0 \right\} \right)$$

In continuation of the effort in determining ***R*** and ***L*** as the distance to a self-clearing cable fault, we developed a method which graphically determines ***R*** and ***L*** on 2-D planes of voltage (v) - current(i) and voltage (v) - current differential (di/dt), respectively, by extracting the zero points of current and current differential. The motivation of the graphical determination is the popularity of 2D barcodes/QR codes and improved image processing capabilities available on hand-held devices on which our method can be implemented on application platforms. Upon such an implementation, image sensor-equipped, hand-held devices such as smartphones and tablets can perform on the spot fault location estimation in real time. The method has been validated with simulated faults on the ATP/EMTP platform [6], [7]. The present paper investigates, applying the graphical determination approach, the influence of the load distribution in a circuit on the fault location accuracy.

The paper is organized as follows. The next section briefs the graphical algorithm and its fault distance determination method. In Section III, we discuss the ATP modeling/simulation process under the different load configurations and load profiles. Section IV focuses on the result of the graphical algorithm under multi-spatial loads. Section V concludes the paper.

## II. Graphical Determination Of Location For Self-Clearing Transient Fault

### *A. Transient Fault Location Formulation*

Fig. 1 depicts a final, reduced system circuit consisting of the path of a faulted phase A from the substation to a fault point *x*. This circuit is the result of a breakdown of a 3-phase setup by the application of the concepts of net fault voltage and current, negative voltage injection and the superposition principle assuming that system or bus voltages are approximately equal for pre-fault and during fault periods [1]-[4]. It is further assumed that there is zero fault resistance between the cable conductor and its concentric neutral.

The above stipulations coupled with a breakdown of the fault voltage and current loops within the reduced circuit shown in Fig. 1, lead to the derivation of key equations that combine to make the final formula.

In Fig. 1, $\Delta \boldsymbol{i}$, $\boldsymbol{i_{CF}}$, $\boldsymbol{i_{RLF}}$ and $\boldsymbol{v_{LS}}$ represent net fault currents and voltages respectively contributed only by the injected voltage source (simulating the short circuit between the faulted point and the neutral). Data measurements made by CTs and PTs at central points, in this case the substation level, capture pre-fault and during fault data. The net fault quantities are simply

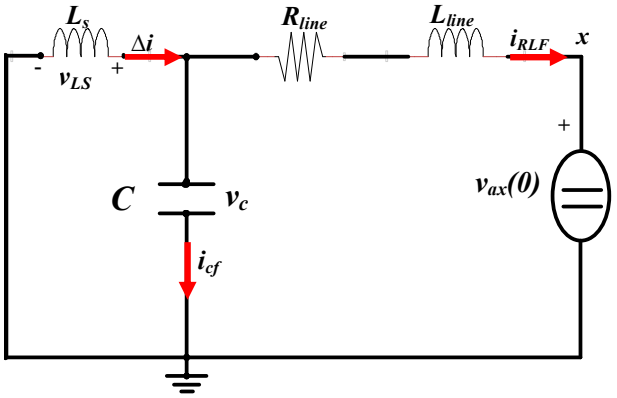


Fig. 1. Final reduced circuit diagram of a Phase A S-L-G fault.

obtained by subtracting the normal, pre-fault values from those measured during the fault period. Also, the amount of negative voltage, injected at *x*, is estimated to be the value of the measured voltage at the fault inception time $t = 0$ or $t = tF$. Due to the application of superposition, the source voltage is removed leaving the injected voltage, $\boldsymbol{v_{ax}(0)}$ or $\boldsymbol{v_{ax}(tF)}$ between *x* and ground in the reduced circuit.

From Fig. 1, the following equations are derived:

$$R_{line} = \frac{V(tF) - v_{LS} - L_{line}\left( \frac{d\Delta i(t)}{dt} - C\frac{d^2 v_c(t)}{dt} \right)}{\Delta i - C\left( \frac{dv_c(t)}{dt} \right)} \quad (1)$$

$$L_{line} = \frac{V(tF) - v_{LS} - R_{line}\left( \Delta i - C\frac{dv_c(t)}{dt} \right)}{\frac{d\Delta i(t)}{dt} - C\left( \frac{d^2 v_c(t)}{dt} \right)} \quad (2)$$

where $\frac{d^2 v_c(t)}{dt}$ is the second derivative of the net fault voltage.

Owing to its small value, the source inductance, $L_s$, is ignored therefore the drop, $\boldsymbol{v_{LS}}$, is no longer considered. Also, in the absence of a capacitor bank, the following final fault distance equations are drawn:

$$R_{line} = \frac{V(tF) - L_{line}\left( \frac{d\Delta i(t)}{dt} \right)}{\Delta i} \quad (3)$$

$$L_{line} = \frac{V(tF) - \Delta i(R_{line})}{\frac{d\Delta i(t)}{dt}} \quad (4)$$

where $\boldsymbol{V(tF)}$ [$\boldsymbol{v_{ax}(0)}$] is value of voltage at the measurement point during the onset of the fault.

*B. Graphical Determination Method*

From equations (3) and (4), line inductance and line resistance to the fault location $\boldsymbol{x}$ can be computed. To enable these computations, however, specific parameter inputs are required as can be seen from both equations. Before these necessary inputs are considered, a final manipulation of equations (3) and (4) must be carried out to implement a graphical determination method.

Evaluating the derivations made in (3) and (4), two important assertions are made which highlight the graphing system and how points are extracted thereof. At $\frac{d\Delta i(t)}{dt} = 0$ in (3), the drop due to the inductance of the line disappears leaving the simplified formula:

$$R_{line} = \frac{V(tF)}{\Delta i} \tag{5}$$

Similarly, at $\Delta \boldsymbol{i} = 0$ in (4), the resistance of the line disappears leaving the simplified formula:

$$L_{line} = \frac{V(tF)}{\left(\frac{d\Delta i(t)}{dt}\right)} \tag{6}$$

Applying (5) and (6), therefore, represents two plots: (a) a plot of $\boldsymbol{V}$ and $(\frac{d\Delta i}{dt})$ both on the vertical axis against $\Delta \boldsymbol{i}$ on the horizontal axis and (b) a plot of $\boldsymbol{V}$ and $\Delta \boldsymbol{i}$ both on the vertical axis against $(\frac{d\Delta i}{dt})$ on the horizontal axis. A setup of these graphs allows for line parameter loci at zero crossings to be extracted as illustrated in Fig. 2 for fault location by R ($R_x$ = A/B) and in Fig. 3 for fault location by L ($L_x$ = C/D).

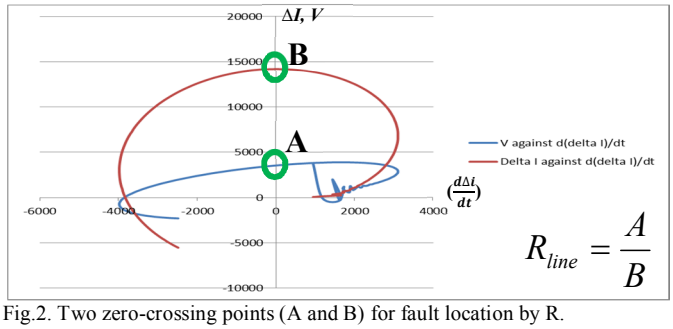


Fig.2. Two zero-crossing points (A and B) for fault location by R.

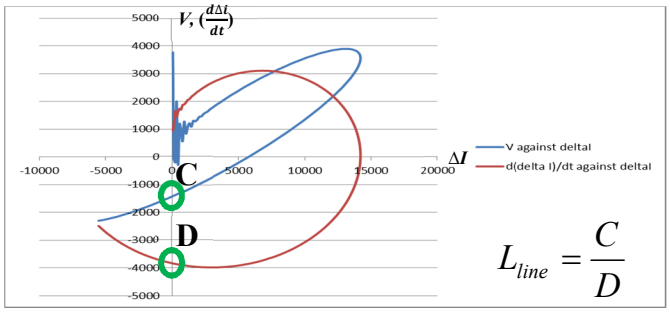


Fig.3. Two zero-crossing points (C and D) for fault location by L.

*C. Method of Graphing from Time-Domain Data*

As can be seen from the graphical determination of fault location, mapping out characteristic plots and extracting necessary inputs requires processing of fault voltage and current waveform data. We hereby describe how graphing is done from fault waveform data. Data obtained from monitoring points at the substation level contain raw voltage and current values synchronized with timestamps and involve pre-fault and during fault data.

The net fault values are computed from a synchronized, sample by sample difference calculation between the normal, pre-fault values and the fault values over the duration of the fault [1]-[4]. In the case of the time derivative of the net fault current, a numerical differentiation method known as the finite difference method is used based on the proximity of data points and how evenly spaced they are [6]. The finite difference method is given by: $(\frac{d\Delta i}{dt}) = \frac{\Delta i(n+1) - \Delta i(n)}{t_{n+1} - t_n}$

The graphing process for line parameter curves involves a selection of matching data points. Since two separate 2D graphs will have to be drawn in order to extract zero-crossing points for $\boldsymbol{R}$ or $\boldsymbol{L}$, we, as a result, need a total of four (4) sub-plots to make out the two initial plots; one initial plot for $\boldsymbol{R}$ and the other for $\boldsymbol{L}$ calculations. The four sub-plots include: (a) Fault voltage against time derivative of the net fault current $(\frac{d\Delta i}{dt})$; (b) Net fault current, $\Delta \boldsymbol{i}$, against time derivative of the net fault current $(\frac{d\Delta i}{dt})$; (c) Fault voltage against net fault current, $\Delta \boldsymbol{i}$; (d) Time derivative of the net fault current $(\frac{d\Delta i}{dt})$ against the net fault current, $\Delta \boldsymbol{i}$.

The first two sub-plots (a) and (b) are superposed together to make out the zero-crossing points **A** (from sub-plot (a)) and **B** (from sub-plot (b)) for fault location determination by $\boldsymbol{R}$. Fig. 4 shows the two sub-plots of (a) and (b). Similarly, sub-plots (c) and (d), when superposed together, make out the zero-crossing points **C** (from sub-plot (c)) and **D** (from sub-plot (d)) for fault location by $\boldsymbol{L}$. Fig. 5 shows sub-plots (c) and (d).

In order to pinpoint the zero crossings, the graphical approach considers four interpolation methods including forward, backward, linear and cubic spline and adopts the one with best result considering the range of values within which the zero-crossing points lie.

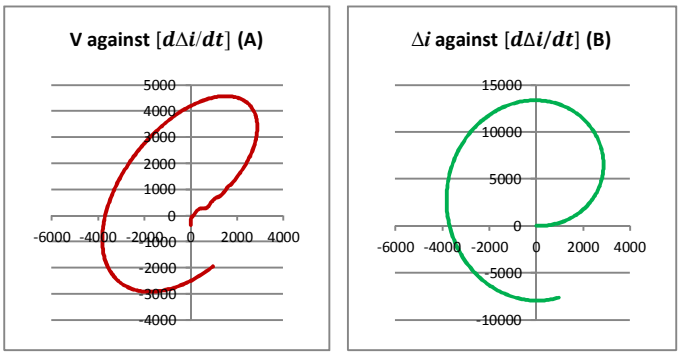


Fig. 4. Sub- plots (a) and (b) for final input parameter extraction for *R*

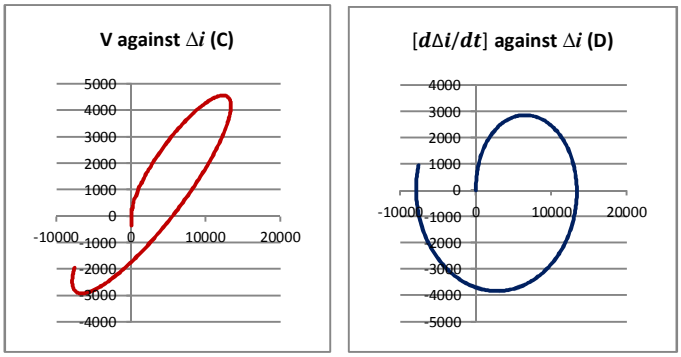


Fig.5. Sub-plots (c) and (d) for final input parameter extraction for *L*

## III. Fault Simulation And Load Configuration

Staged transient faults under different load locations with respect to fault locations are simulated with ATP/EMTP, a universal program for digital simulation of transient phenomena [7] in conjunction with a graphical, mouse-driven preprocessor known as ATPDraw [8]. The simulation involves the following four steps: distribution system design, underground cable modeling, multi-spatial load distribution design, and staged transient fault simulation.

### *A. Distribution System Configuration*

A similar simplified system design as seen in [6] is adopted with signal acquisition at the substation (sending end) for a medium voltage distribution network. Fig. 6 shows a sample line design in ATPDraw with a transient fault simulated in between two loads. It involves the following system components and specifications:

- 11kV, 3-phase neutral-grounded ac source with 60Hz frequency
- Source Impedance
- Current and Voltage probes
- An underground cable model (Bergeron)
- 3-phase, Y-grounded loads with series RLC elements.
- The entire system, along with the loads, is arranged so that it maintains close to unity power factor. .

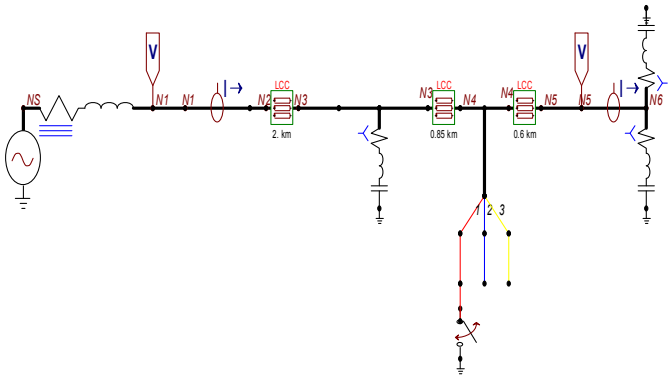


Fig. 6. 3-phase, 11kV distribution system design with 3-phase loads

### *B. Cable Modeling*

A BERGERON model, which is a simple, constant frequency method, is used for the underground cable system [7]-[9]. For a 3-phase system connection, 3 conducting cables are used where each cable represents a phase in the distribution system. The system frequency is set at 60Hz throughout the modeling and simulation process. Fig. 7 and Table I show the configuration and material properties of the modeled cable respectively.

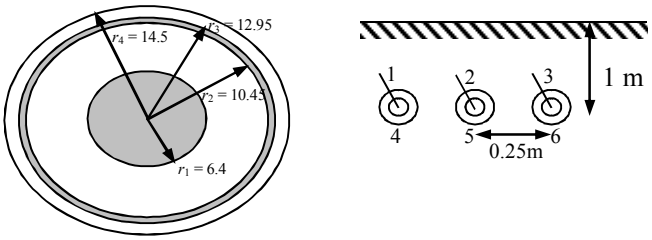


Fig. 7. Cable configuration and geometric properties (Units on the left in mm)

TABLE I
UNDERGROUND CABLE MATERIAL PROPERTIES

| **Specification of MV underground cable material** (XLPE Stranded Copper Conductor, Bergeron Model) | |
|---|---|
| **Core Conductor** | $\rho_c$ = 1.7E-8 Ωm , $\mu_c$ = 1.0 |
| **Insulation** | $\varepsilon_i$ = 2.7 , $\mu_i$ = 1.0 |
| **Sheath** | $\rho_{sh}$ = 2.5E-8 Ωm , $\mu_{sh}$ = 1.0 |

where $\rho_c$ = core resistivity, $\mu_c$ = core relative permeability, $\rho_{sh}$ = sheath resistivity, $\mu_{sh}$ = sheath relative permeability, $\varepsilon_i$ = insulation relative permittivity and $\mu_i$ = insulation relative permeability

With the above arrangement and a subsequent use of a method involving sequence component (**SC**) to phase component conversion [6]–[10], the preset circuit parameters are obtained. Sample preset parameters with two fault locations are listed in Table II.

TABLE II
PRESET CIRCUIT PARAMETERS

| **Fault Distance [km]** | **$R_{line}$ [Ω]** | **$L_{line}$ [mH]** |
|---|---|---|
| 1.25 | 0.3103325 | 0.4443075 |
| 2.5 | 0.620665 | 0.888615 |

### *C. Multi-spatial Load Distribution*

To extensively test the performance of the algorithm, three separate load profiles are used with each profile being significantly different from the others while sub-cycle, transient faults are simulated at various points on the cables connecting these loads. The loads are modeled as series RLC elements connected in parallel along the distribution feeder; however, L and C values are set very low so that the RLC element looks more like an R element. Table III summarizes the three load profiles. Fig. 8 shows the system setup with each of the load profiles.

TABLE III
LOAD PROFILES

| | From Sending End | | | |
|---|---|---|---|---|
| **Load Profile No.** | **Load 1 (Series RLC)** | **Load 2 (Series RLC)** | **Load 3 (Series RLC)** | **Load 4 (Series RLC)** |
| **1** | R = 240 Ω<br>L = 132.63 mH<br>C = 53.052 µF | R = 240 Ω<br>L = 132.63 mH<br>C = 53.052 µF | N/A | N/A |
| **2** | R = 240 Ω<br>L = 132.63 mH<br>C = 53.052 µF | R = 500 Ω<br>L = 132.63 mH<br>C = 53.052 µF | R = 360 Ω<br>L = 132.63 mH<br>C = 53.052 µF | R = 120 Ω<br>L = 132.63 mH<br>C = 53.052 µF |
| **3** | R = 240 Ω<br>L = 132.63 mH<br>C = 53.052 µF | R = 500 Ω<br>L = 132.63 mH<br>C = 53.052 µF | R = 360 Ω<br>L = 132.63 mH<br>C = 53.052 µF<br>R = 240 Ω<br>L = 132.63 mH<br>C = 53.052 µF | R = 120 Ω<br>L = 132.63 mH<br>C = 53.052 µF |

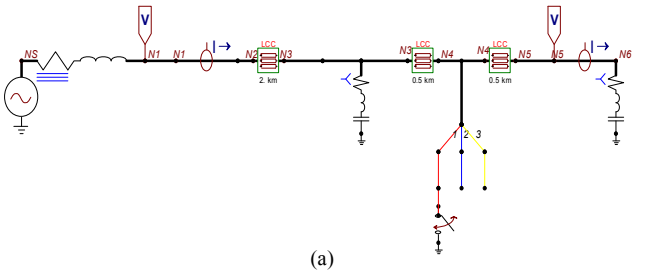

(a)

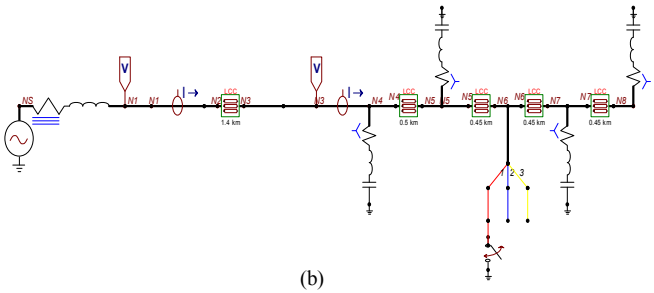

(b)

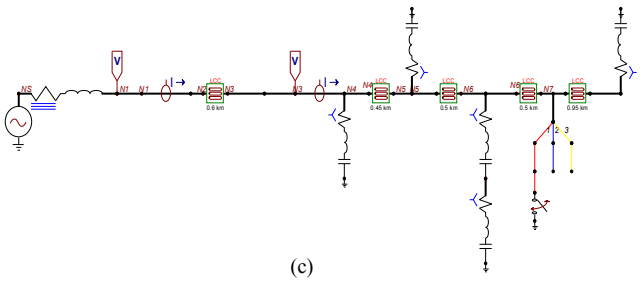

(c)

Fig. 8. System setup showing connected RLC loads: (a) Load Profile 1, (b) Load Profile 2, and (c) Load Profile 3.

Under each profile, a fault is initiated along a section of the line joining any two chosen loads.

### *D. Transient Fault Simulation*

During each staged fault under different a load configuration, voltage and current probes are mounted at the sending end of the circuit to pick up discrete normal and during fault signals at 15360 samples per second. Simulations are run at five (5) separate distances; two being run on load profile 1, the next two on load profile 2 and the final distance being simulated on load profile 3. For each fault simulation, the fault duration is set between 0.0125 seconds (fault inception) - 0.0292317 (fault ending) seconds, with a simulation time step of 5 micro-seconds at 60Hz power cycle.

TABLE IV
SETUP FOR SIMULATION

| **Fault Type** | Transitory Single-Line-To-Ground fault | |
|---|---|---|
| **Fault Inception Time – Fault Clearance Time** | 0.0125 - 0.0292317 secs | |
| **Fault Distance** | Load Profile 1 | 1.25 km from sending end |
| | | 2.5 km from sending end |
| | Load Profile 2 | 2.35 km from sending end |
| | | 3.5 km from sending end |
| | Load Profile 3 | 2.05 km from sending end |

Time-domain data generated from each simulation is used to generate the four sub-plots which are then used to extract the zero-crossing points necessary for fault distance calculation. The next section discusses the results and outlines any observations made.

## IV. RESULTS AND VALIDATION

As indicated earlier, five different simulations are run with each corresponding to a particular load profile and a specific fault inception point. Validation is done with respect to the preset parameters. Table IV summarizes the initial results from our algorithm as compared with the preset values generated prior to simulation. Table V shows the percentage error margins.

From Table V, the accuracy of the 2D graphical algorithm seems to generally stay within acceptable limits especially with the fault distance by resistance values. The fault distance by the inductance estimation, on the other hand, shows relatively higher error. As a general observation from prior work [6] and this one, however, the accuracy of the method seems to be mostly impacted by increasing length of the fault location. To better show the impact of the different load profiles, comparison simulations are run under each load profile keeping the distance to fault inception point the same. Three distances (1.8 km, 2 km and 2.5 km) are used for each set of simulations. Fig. 9 and Fig. 10 show the fault distances by resistance and inductance values respectively under each fixed inception point. The preset line parameter values are also provided to serve as points of reference.

TABLE IV
PRELIMINARY RESULTS FOR FAULT DISTANCES

| Sim No. (fault distance) | Load Profile Number | Preset Distance $R_{line}$[Ω] | Calculated Distance $R_{line}$[Ω] | Preset Distance $L_{line}$ [mH ] | Calculated Distance $L_{line}$ [mH] |
|---|---|---|---|---|---|
| **11** (1.25 km) | 1 | 0.31033 | 0.313862 | 0.44431 | 0.467114 |
| **12** (2.5 km) | 1 | 0.62067 | 0.62871 | 0.88862 | 0.93887 |
| **13** (2.35 km) | 2 | 0.58343 | 0.591188 | 0.83529 | 0.9022091 |
| **14** (3.5 km) | 2 | 0.86893 | 0.882657 | 1.24406 | 1.355774 |
| **15** (2.05 km) | 3 | 0.50895 | 0.515014 | 0.72866 | 0.783481 |

TABLE V
PERCENTAGE ERROR FOR LINE PARAMETERS

| Simulation Number (fault distance) | Load Profile Number | Error between Preset $R_{line}$ vs. Calculated Distance in $R_{line}$ (%) | Error between Preset $L_{line}$ vs. Calculated Distance in $L_{line}$ (%) |
|---|---|---|---|
| **11** (1.25 km) | 1 | 1.137360734 | 5.13311164 |
| **12** (2.5 km) | 1 | 1.295803694 | 5.655024955 |
| **13** (2.35 km) | 2 | 1.330573539 | 8.01043364 |
| **14** (3.5 km) | 2 | 1.579676637 | 8.979720448 |
| **15** (2.05 km) | 3 | 1.192407121 | 7.522901836 |

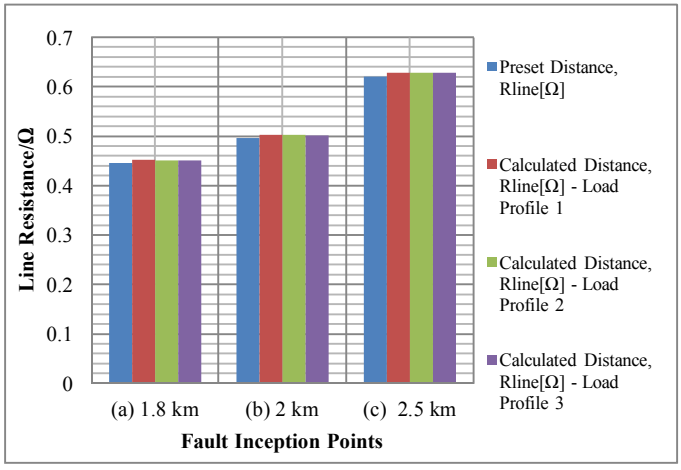


Fig. 9. Comparison charts of $R_{line}$ under fixed fault inception points for Load Profiles 1, 2 and 3

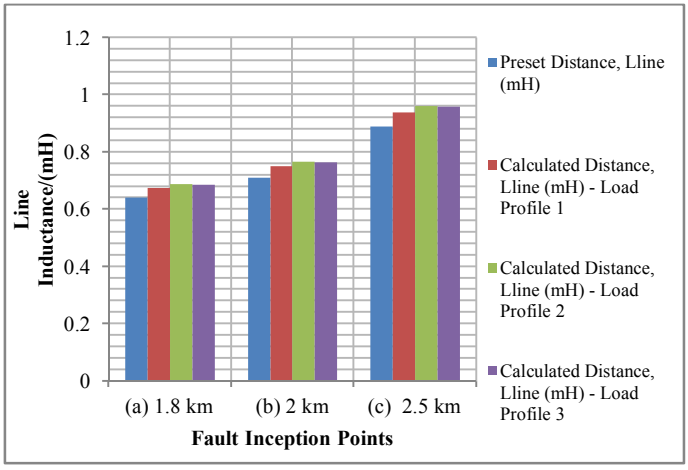


Fig. 10. Comparison charts of $L_{line}$ under fixed fault inception points for Load Profiles 1, 2 and 3

From the comparison charts above, it can be observed that the calculated parameters are in close proximity to the preset values regardless of what load profile is used. As mentioned earlier, the fault distance by inductance estimation shows a relatively higher error margin which is also observed under the consideration with a fixed inception point. Furthermore, in relation to the corresponding error margins, the absolute percentage error for resistance estimations remained at approximately 1.3% for each of the fixed points. However, it is observed by way of inductance estimation that the error was relatively lower (approx. 5%) under load profile 1 and slightly higher (between 7% and 8%) under load profiles 2 and 3 for each of the three fixed inception points. Overall, the distance of the fault location seems to be the biggest factor that impacts accuracy of the 2D graphical algorithm as load configuration and load center location showed minimum impact.

## V. CONCLUSION

This paper described is a continued work for self-clearing fault location in underground cables. The focus of this work was to investigate the impact of fault location with respect to the load center location for a hitherto developed 2D graphical algorithm. It used the extraction of parameter loci at zero-crossing points of the fault loop as well as those of its time derivative as inputs for a distance formula. These inputs were used to determine the location of a fault in terms of resistance and inductance. To test the impact of multi-spatial loads and load center location, three load profiles were modeled, and faults were simulated at different sections of the cables connecting the loads. Results of the tests were validated with preset circuit values. In general, the algorithm proved resilient and adaptable to different load types and center locations. Slight variations in accuracy were observed but they were not

significant enough to impact the general efficacy of the method.

## REFERENCES


[1] Charles Kim and Thomas Bialek, "Sub-cycle Ground Fault Location – Formulation and Preliminary Results", *2011 IEEE Power Systems Conference & Exposition*, March 20-23, 2011

[2] Charles Kim, Tom Bialek, Matti Lehtonen, and Mohamed Abdel-Fattah, "Location of Underground Cable Transitory Faults," 2011 International Conference of Power System Transients (IPST), Delft, The Netherlands, June 14-17, 2011.

[3] Charles Kim, Thomas Bialek and Jude Awiylika, "An Initial Investigation for Locating Self-Clearing Faults in Distribution Systems", *IEEE Transactions of Smart Grid,* vol. 4, no. 2, pp. 1105-1112, June 2013.

[4] Charles Kim, "Apparatus and Method for Fault Detection and Location Determination," U. S. Patent 8941387 (January 27, 2015)

[5] Charles Kim, Locating Transient Faults in Distribution Feeder - Feasibility Study on Anticipation and Predictive Location of Distribution Cable Faults, Report-SDGE, September 2015.

[6] Derrick Anang and Charles Kim, " Graphical Determination of Transient Cable Fault Location with Captured Time-Domain Data," A paper submitted to IEEE North American Power Symposium, September 2018

[7] Electromagnetic Transients Program (EMTP) Theory Book, July 1995.

[8] László Prikler and Hans Kristian Høidalen. "ATPDraw User Manual" v.3.5, October, 2002

[9] Neville Watson and Jos Arrillaga, "Power Systems Electromagnetic Simulation – IET Power and Energy Series 39*",* 2007.

[10] Akihiro Ametani, Teruo Ohno and Naoto Nagaoka, "Cable System Transients: Theory, Modeling and Simulation", *IEEE Press,* John Wiley & Sons Singapore Pte. Ltd., 2015.


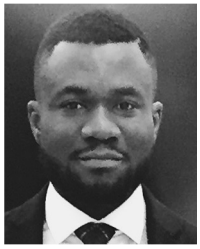

**Derrick S. Anang** received his B.Sc.(EE) degree from Kwame Nkrumah University of Science and Technology (K.N.U.S.T), Kumasi, Ghana, in 2013 and M.Eng.(EE) degree from Howard University, Washington, DC, in 2016. He is currently pursuing a Ph.D. degree in EE at Howard University, Washington, DC with research areas in transient fault location in distribution systems and optimization and reliability studies for HEMT devices in power electronic boards.

**Charles Kim** (M'90–SM'06) received the Ph.D. degree in electrical engineering from Texas A&M University, College Station, TX, in 1989 in the subject area of power system automation and high impedance fault in distribution systems. Currently, he is a Professor in the Department of Electrical Engineering and Computer Science at Howard University, Washington, DC. His research interests include failure detection, anticipation, and prevention in safety critical systems. He holds a few U.S. patents in incipient fault location.